Electronic Supplementary Information (ESI) for Journal of Dalton Transactions.
This journal is © The Royal Society of Chemistry 2020

Supporting Information For:

Post-Synthetic Modification of a Metal–Organic Framework with Chemodosimeter for Rapid Detection of Lethal Cyanide via Dual Emission

*Rana Dalapati, Soutick Nandi and Shyam Biswas**

Department of Chemistry, Indian Institute of Technology Guwahati, Guwahati, 781039 Assam, India.

* To whom correspondence should be addressed.
E-mail: sbiswas@iitg.ernet.in. Tel: (+)91-3612583309. Fax: (+)91-3612582349.

Materials and Methods:

The preparation of thieno[2,3-b]thiophene-2,5-dicarboxylic acid (H_2TDC) and 2-cyano-3-(pyren-1-yl)acrylic acid (CPAA) chemodosimeter was carried out by following literature protocols.[1, 2] The ^1H NMR spectra of these ligands are shown in Figures S1-S2. All other reagent grade starting materials were used as received from the commercial suppliers. Perkin Elmer Spectrum Two FT-IR spectrometer was used to record fourier transform infrared (FT-IR) spectra in the region of 400-4000 cm^{-1}. The following indications are used to characterize absorption bands: very strong (vs), strong (s), medium (m), weak (w), shoulder (sh) and broad (br). Thermogravimetric analyses (TGA) were carried out with a Mettler-Toledo TGA/SDTA 851e thermogravimetric analyzer in a temperature range of 30-700 °C under air atmosphere at a heating rate of 5 °C min^{-1}. Ambient temperature X-Ray powder diffraction (XRPD) patterns were measured on a Bruker D2 Phaser X-ray diffractometer operated at 30 kV, 10 mA using Cu-Kα (λ = 1.5406 Å). The nitrogen sorption isotherms up to 1 bar were recorded using a Quantachrome Autosorb iQ-MP gas sorption analyzer at -196 °C. Before the sorption measurements, the compounds were degassed for 12 h under dynamic vacuum at 120 °C. Steady state fluorescence studies were performed with a HORIBA JOBIN YVON Fluoromax-4 spectrofluorometer. DFT calculations were carried out with Gaussian 09 package using 6-31+G (d,p) basis set with B3LYP method.[3]

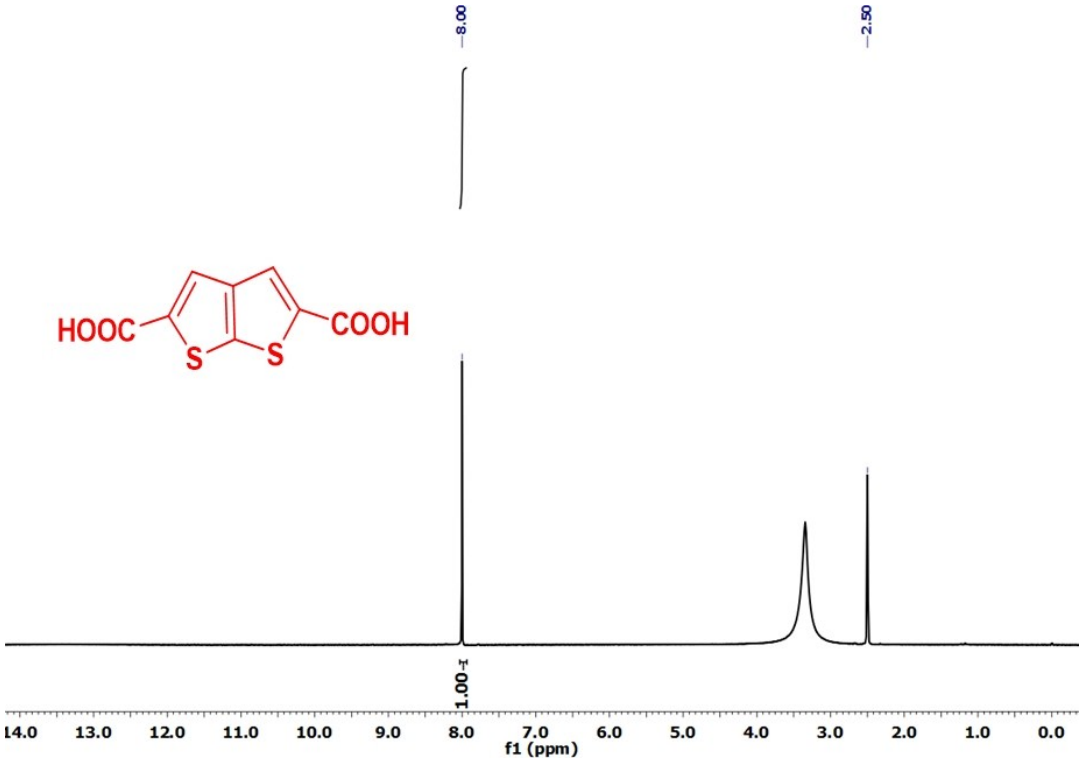

Figure S1. ^1H NMR spectrum of of H_2TDC ligand.

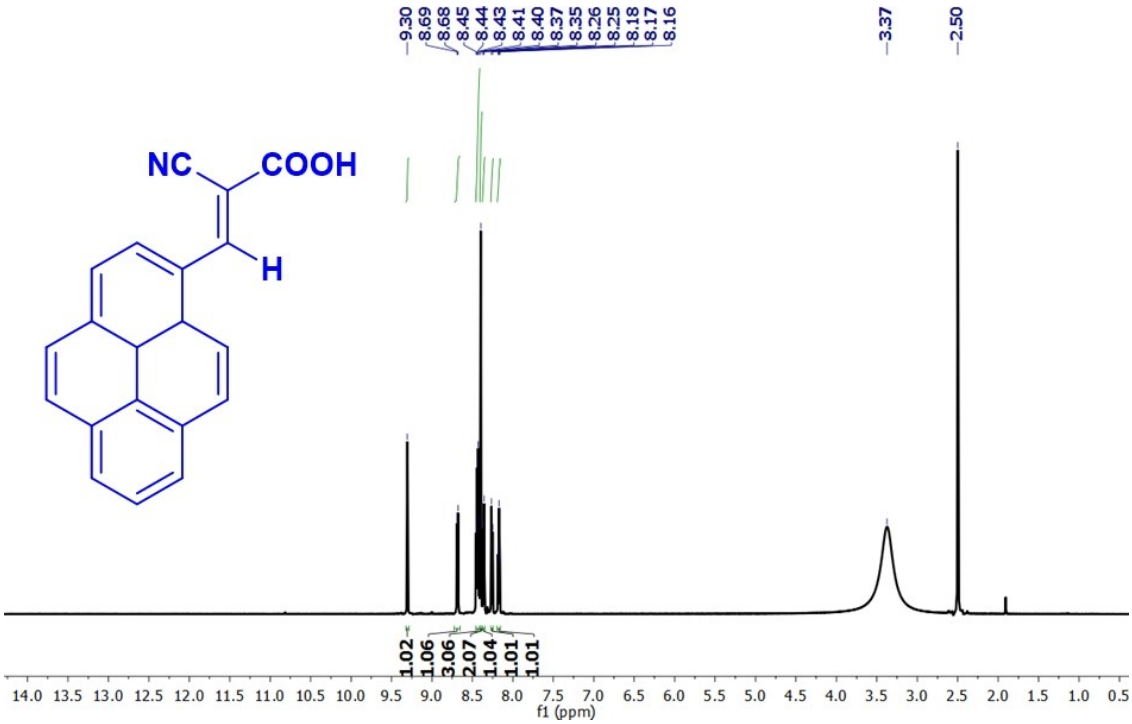

Figure S2. ^{1}H NMR spectrum of of CPAA ligand.

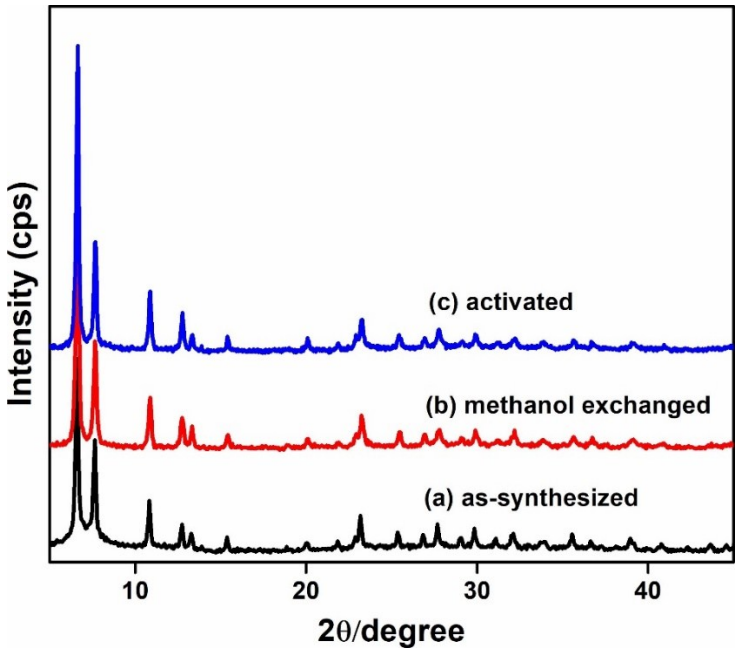

Figure S3. XRPD patterns of as-synthesized (a), methanol exchanged (b) and thermally activated (c) forms of **1**.

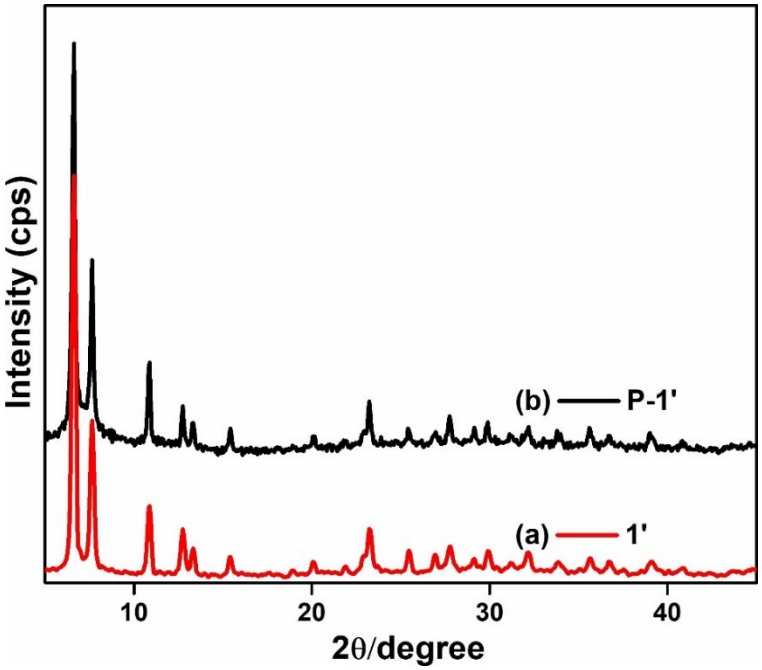

Figure S4. XRPD patterns of **1'** before (a) and after post-synthetic ligand exchange (b).

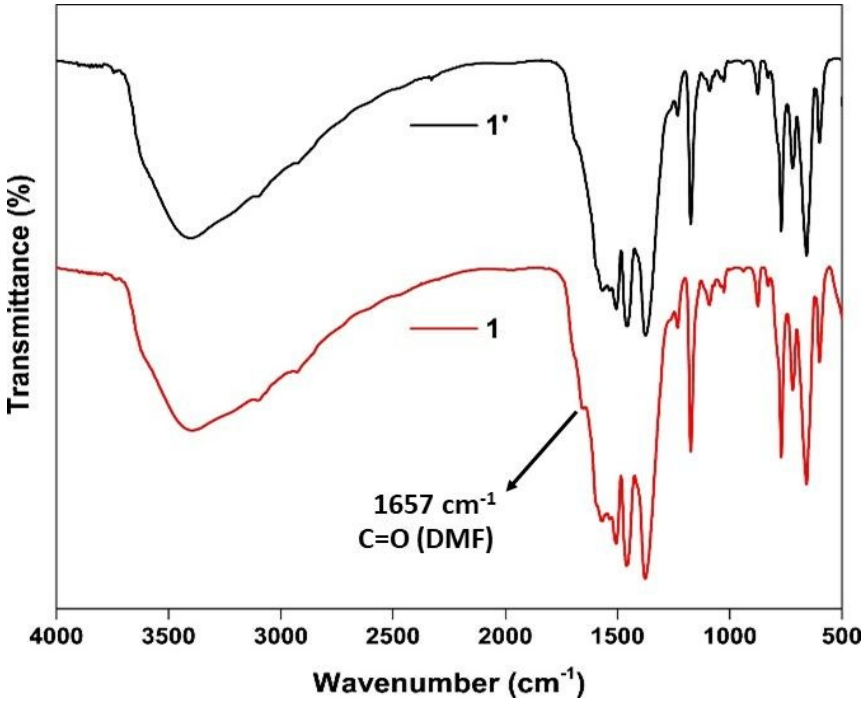

Figure S5. FT-IR spectra of as-synthesized **1** (red) and thermally activated **1'** (black).

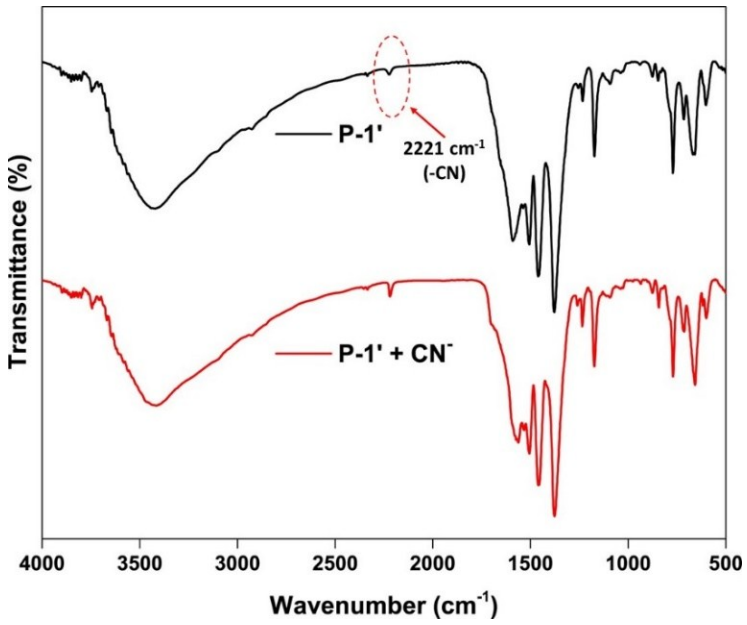

Figure S6. FT-IR spectra of **P-1'** before (black) and after (red) treatment with cyanide.

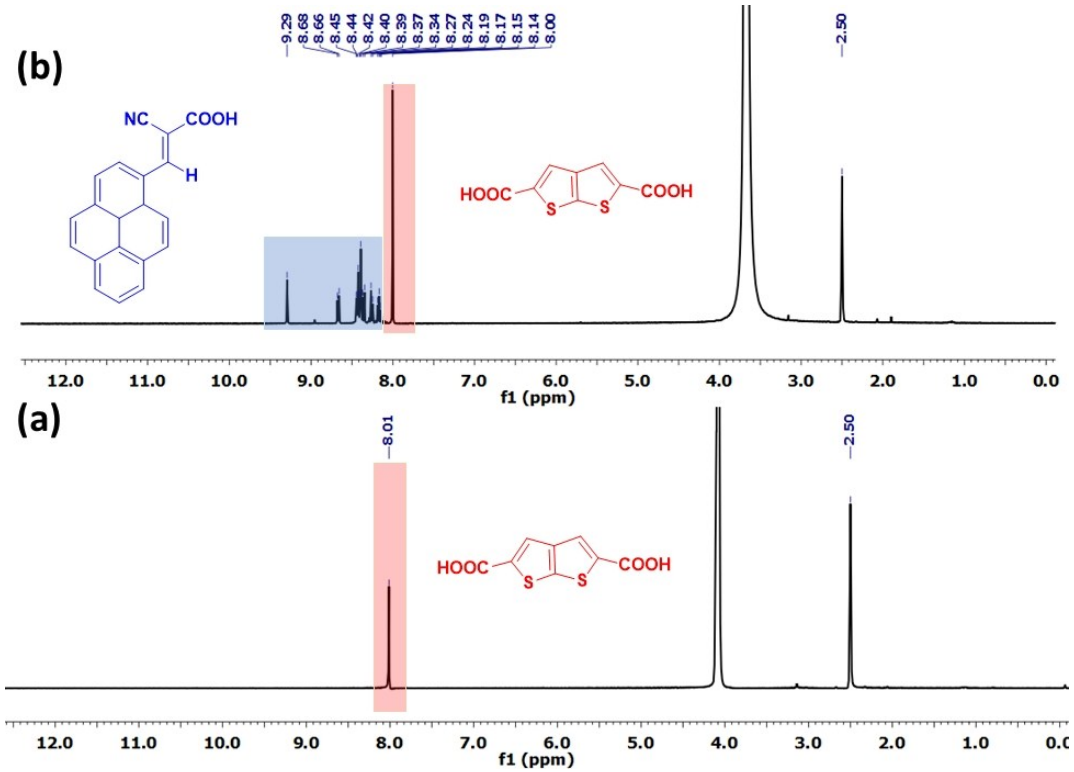

Figure S7. ^{1}H NMR spectra of **1'** (a) and **P-1'** (b) after framework digestion in K_3PO_4/D_2O. In ^{1}H NMR spectrum of digested **P-1'**, presence of the new peaks were observed for the pyrene protons (blue shaded area) along with the proton peaks of H_2TDC ligand (red shaded area).

Digestion protocol: 10 mg of MOF sample was added to 0.5 mL of DMSO-d_6. To this solution was added 0.3 mL of saturated K_3PO_4 in D_2O. After shaking for 10 min, the MOF sample was dissolved and the organic phase was collected and analyzed by ^{1}H NMR spectroscopy.

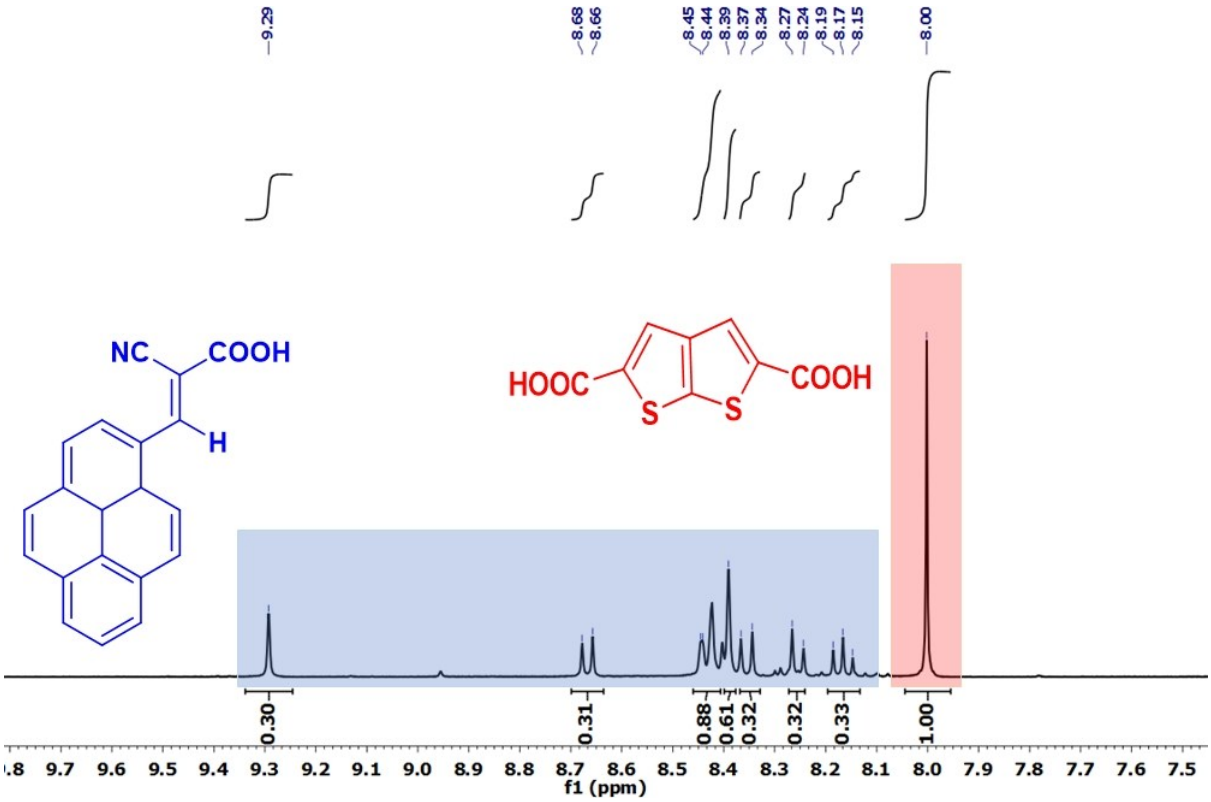

Figure S8. ^{1}H NMR spectrum of **P-1'** after digestion in K_3PO_4/D_2O. To calculate the percent of conversion, the peaks corresponding to H_2TDC ligand was set to an integration of 1 and all new peaks were integrated accordingly. For **P-1'**, these new peaks are all approx. ~0.30 with respect to protons of H_2TDC ligand, corresponding to ~23% incorporation of CPAA ligand in the framework.

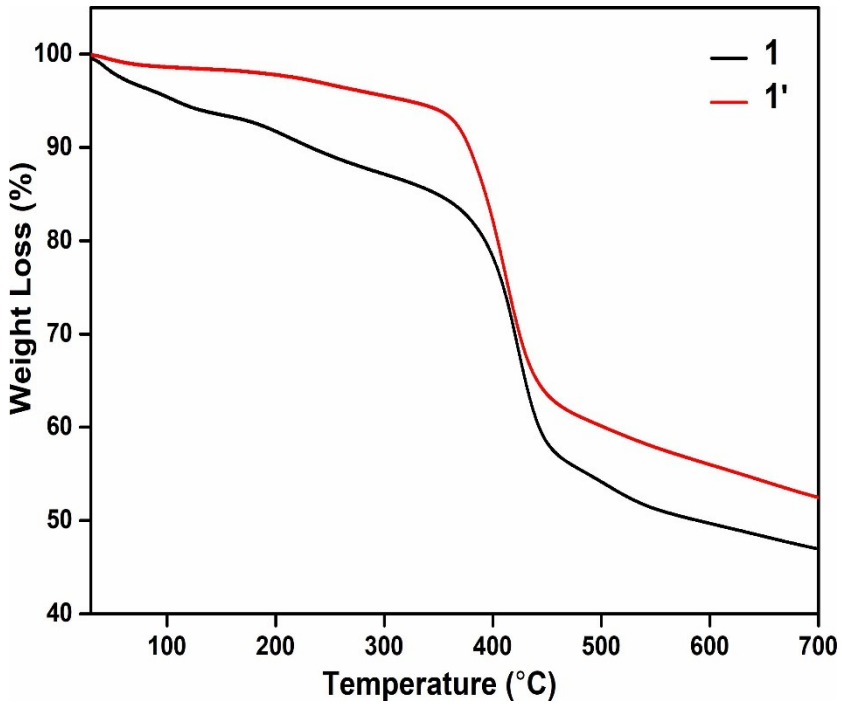

Figure S9. TG curves of as-synthesized **1** (black) and activated **1'** (red) recorded in an air atmosphere in the temperature range of 25-700 °C with a heating rate of 5 °C min^{-1}.

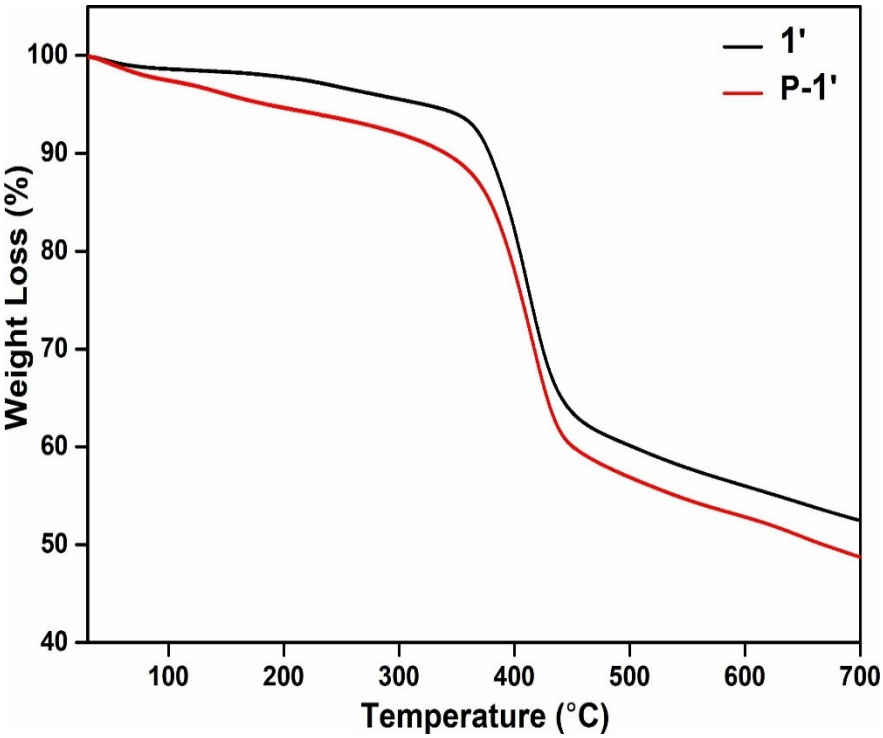

Figure S10. TG curves of **P-1** recorded in an air atmosphere in the temperature range of 25-700 °C with a heating rate of 5 °C min^{-1}.

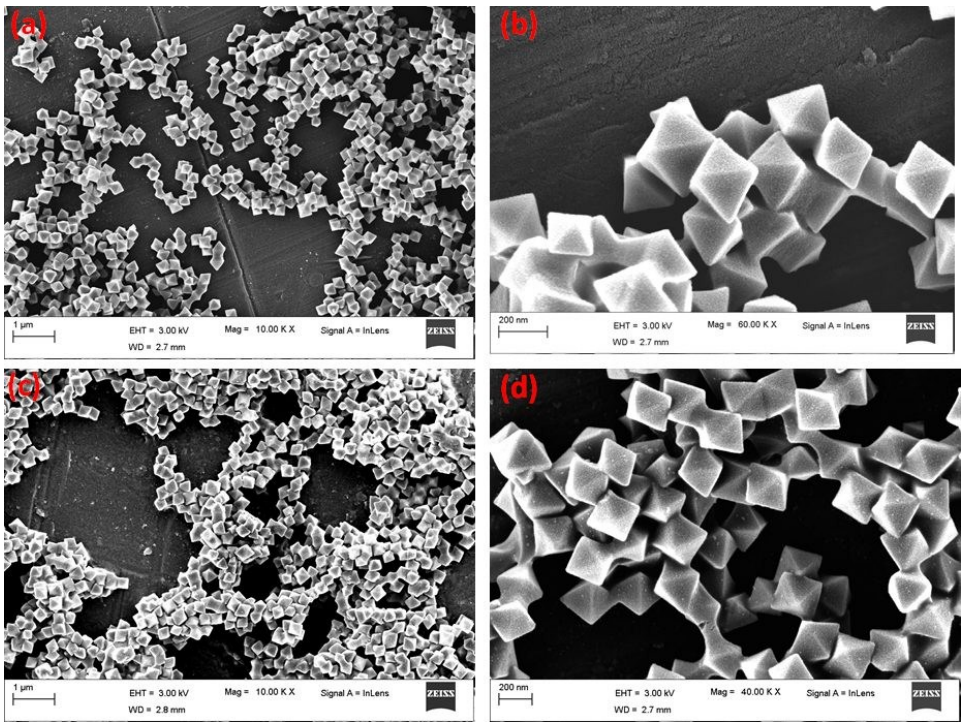

Figure S11. FE-SEM images of **1'** (a, b) and **P-1'**(c, d) in different magnifications.

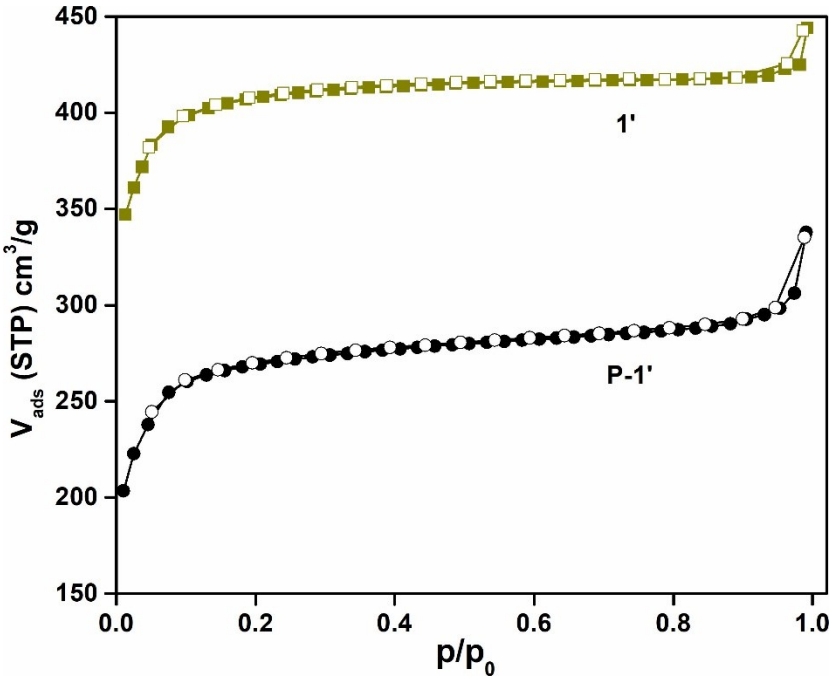

Figure S12. N_2 adsorption (solid symbols) and desorption (empty symbols) isotherms of **1'** (weed green squares) and **P-1'** (black circles) measured at –196 °C.

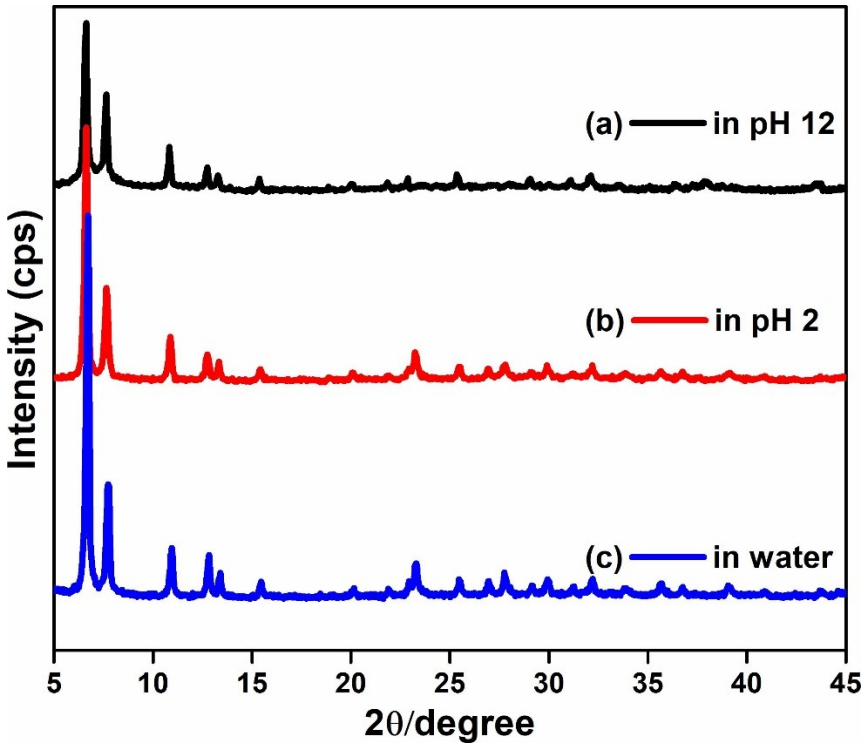

Figure S13. Hydrolytic stability of **P-1'** in different pH media.

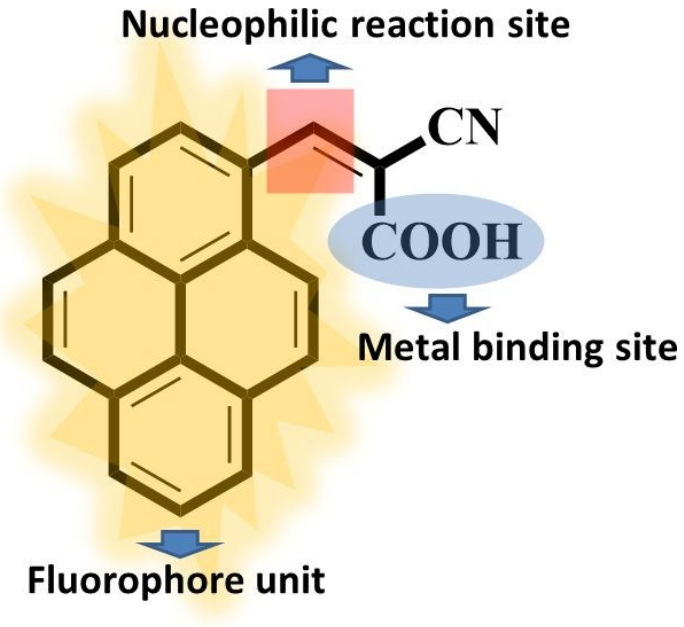

Figure S14. Structure of CPAA probe and its different potential sites.

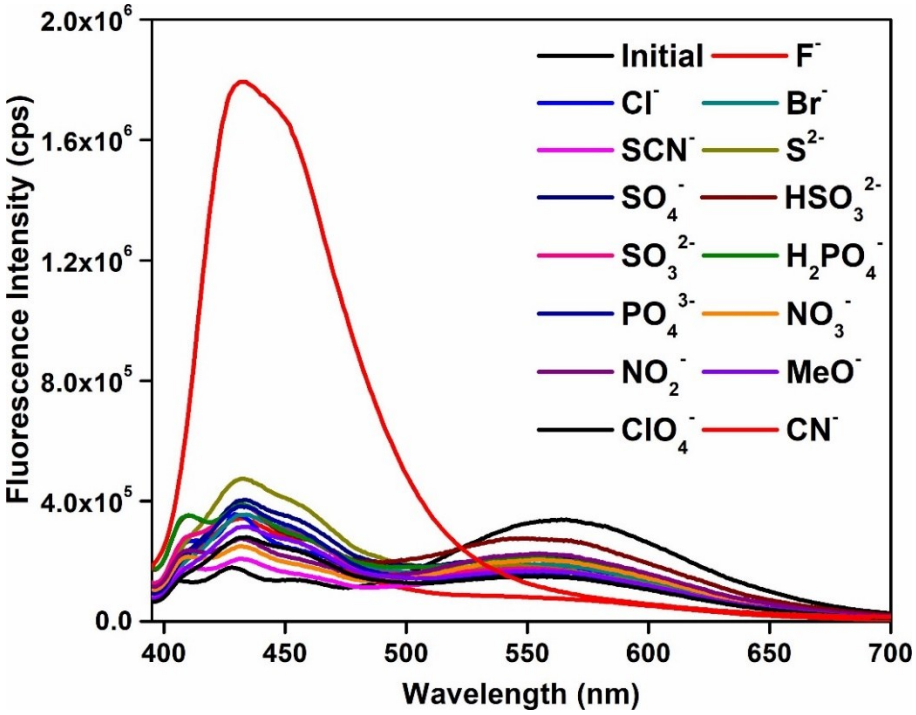

Figure S15. Change in the fluorescence intensity of **P-1'** upon addition of 2 mM aqueous solution (150 µL) of various anions.

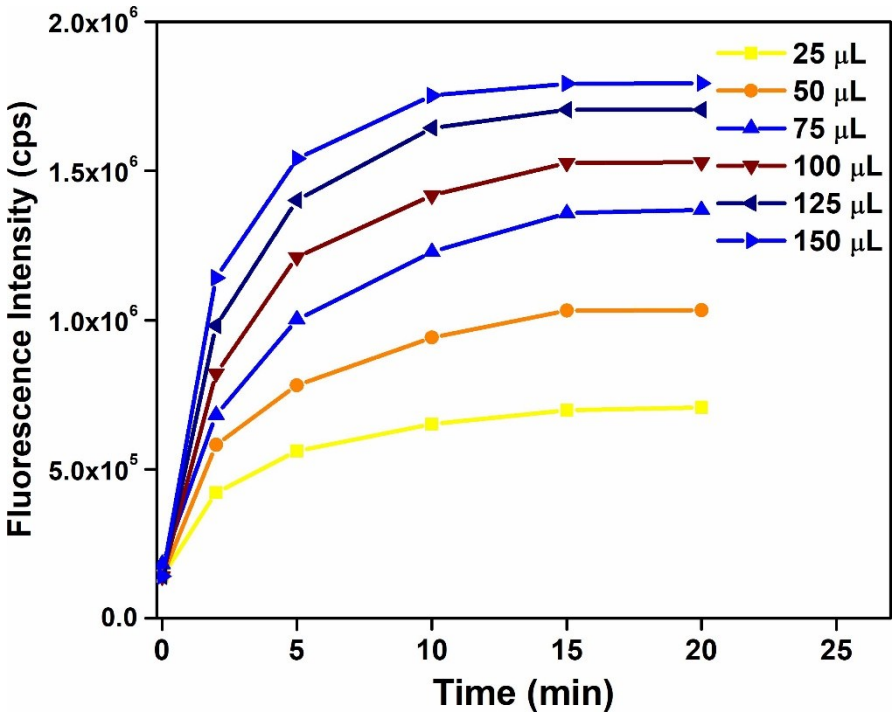

Figure S16. Time-dependent fluorescence enhancement of **P-1'** at 433 nm upon addition of different concentrations of CN^- ion.

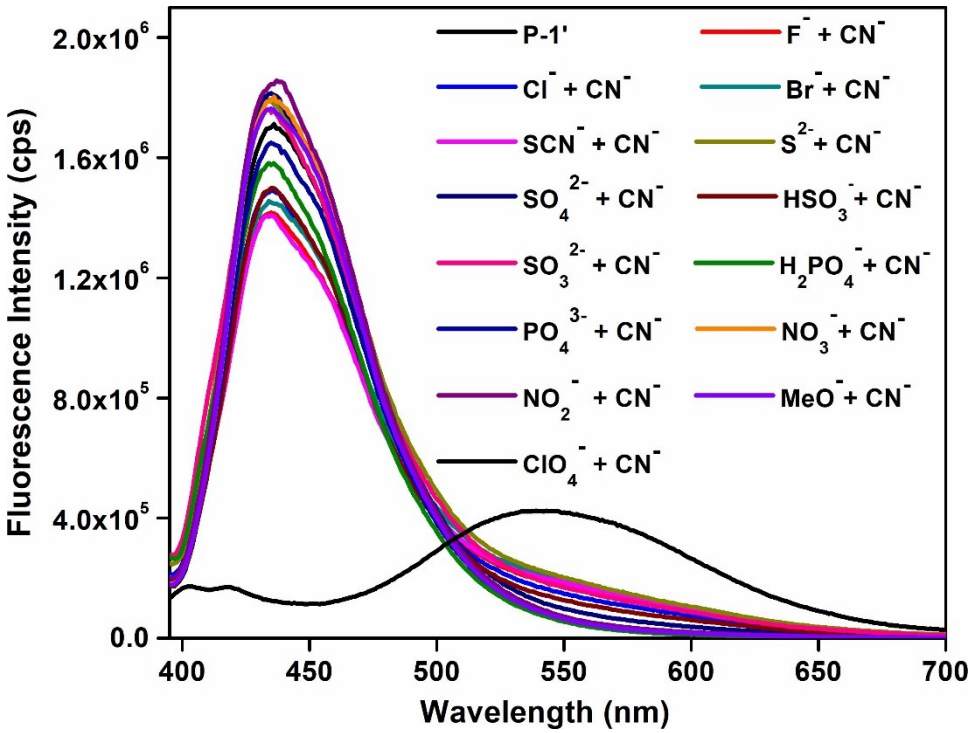

Figure S17. Change in the fluorescence intensity of **P-1'** upon addition of 2 mM CN^- solution (150 μL) in presence of other competitive anions (150 μL).

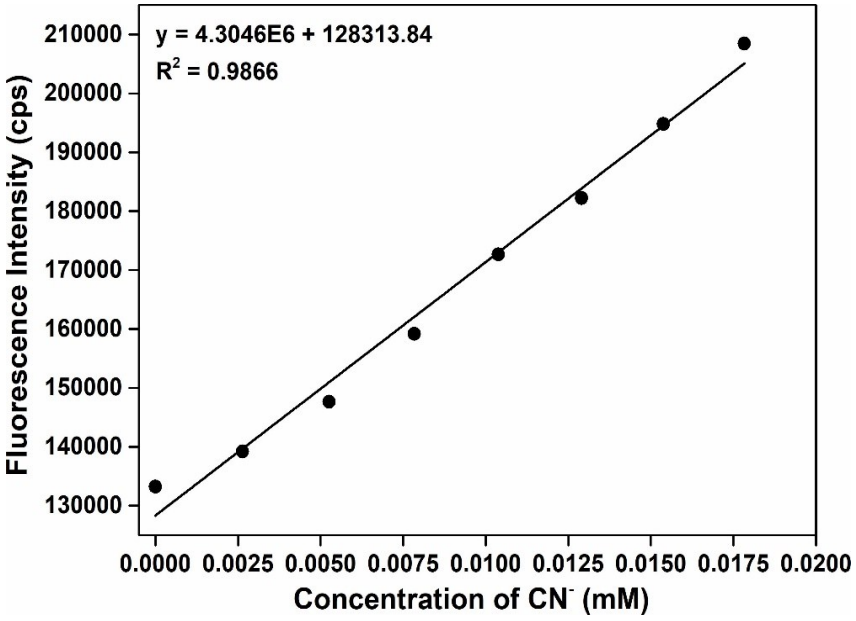

Figure S18. Change in the fluorescence intensity of **P-1'** as a function of CN^- concentration.

Table S1. Comparison of the various existing fluorescent materials for the sensing of CN^-.

Sl No.	Sensor Material	Type of material	Sensing Medium	LOD	Ref.
1	**P-1'**	MOF	THF/ H_2O	0.35 μM	this work
2	CAU-10-N_2H_3	MOF	Water	0.48 μM	4
3	M-ZIF-90	MOF	DMSO/ H_2O	2 μM	5
4	carbazole-functionalized Zr(IV) MOF	MOF	Water	0.14 μM	6
5	Bio-MOF-1⊃DAAC	MOF	HEPES buffer	5.2 ppb	7
6	Tb-ADP-Bipy MOF	MOF	Water	30 nM	8
7	PAT–TFBE	gel	Water	1.82 μM	9
8	BP	Benzo-pyrylium–pheno-thiazine conjugate	CH_3CN/ H_2O	0.13 μM	10
9	NBD-SSH−Cu^{2+}	peptide-based ensemble	Water	24.9 nM	11
10	pyridyl azo-based chemosensor **2**	gel	Sol-gel medium	9.36 μM	12
11	pyridinium-fused	Chemo-dosimeter	THF/ H_2O	54 nM	13

	pyridinone iodide				
12	3T-2CN	Oligo-thiophene chemo-sensor	DMSO/ H_2O	0.19 μM	14
13	AuAgNCs@ ew	bimetallic gold−silver nanoclusters	Water	0.138 μM	15
14	$\{Ru^{II}(^tBubpy)(CN)_4-[Cu^{II}(dien)]_3\}(ClO_4)_2$	trinuclear hetero-bimetallic Ru(II)−Cu(II) complex	DMF/ H_2O	1.2 μM	16
15	receptor **1**	DMN conjugated benzo-thiazole	DMF/H_2O	0.16 μM	17
16	PNA⊃GBP·I_2	Supra-molecular polymer	DMSO–H_2O	41 nM	18

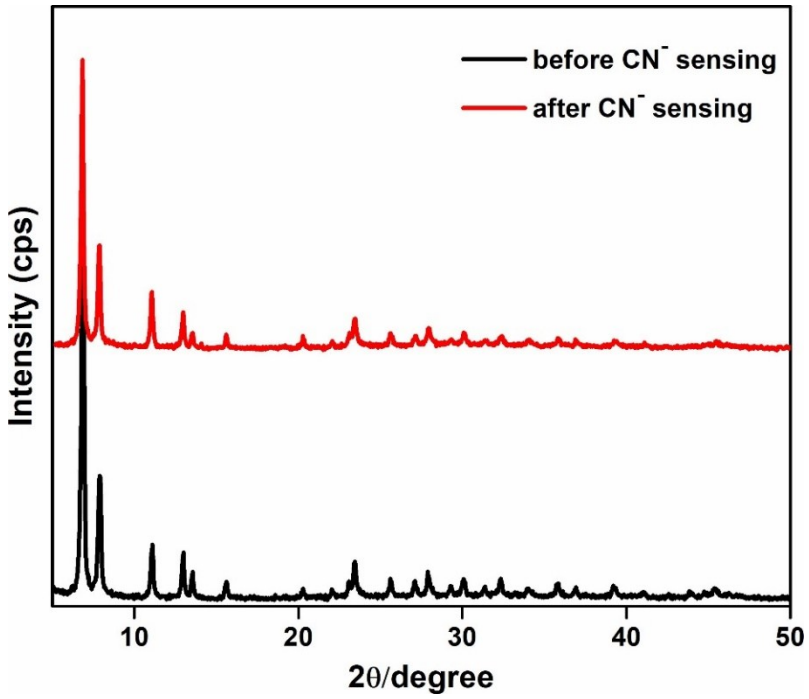

Figure S19. XRPD patterns of **P-1'** before (a) and after (b) cyanide sensing.

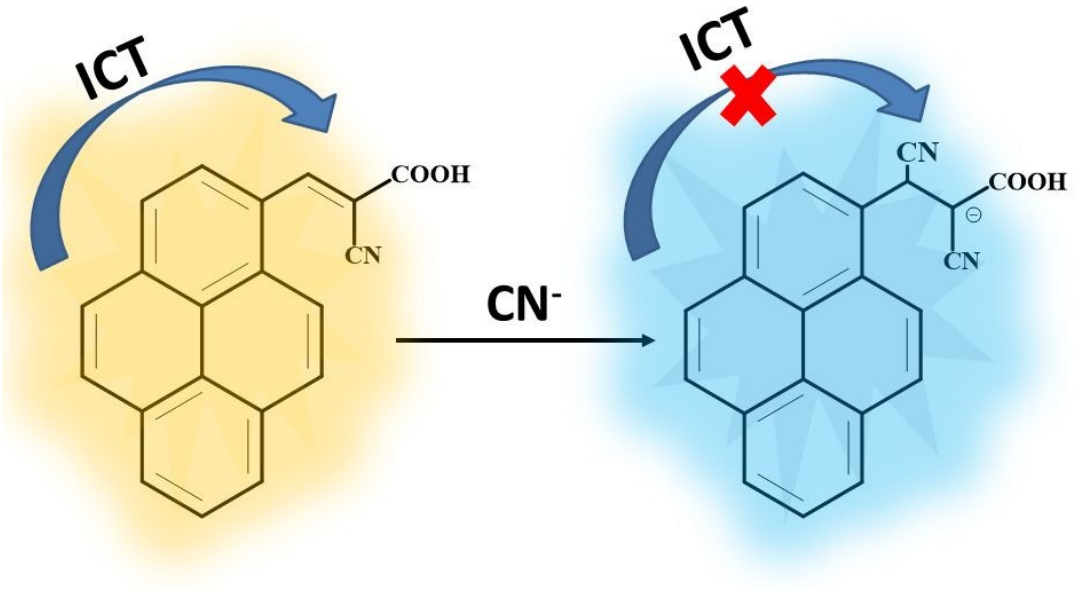

Figure S20. Suppression of ICT (intramolecular charge transfer) due to addition of cyanide ion to the CPAA probe.

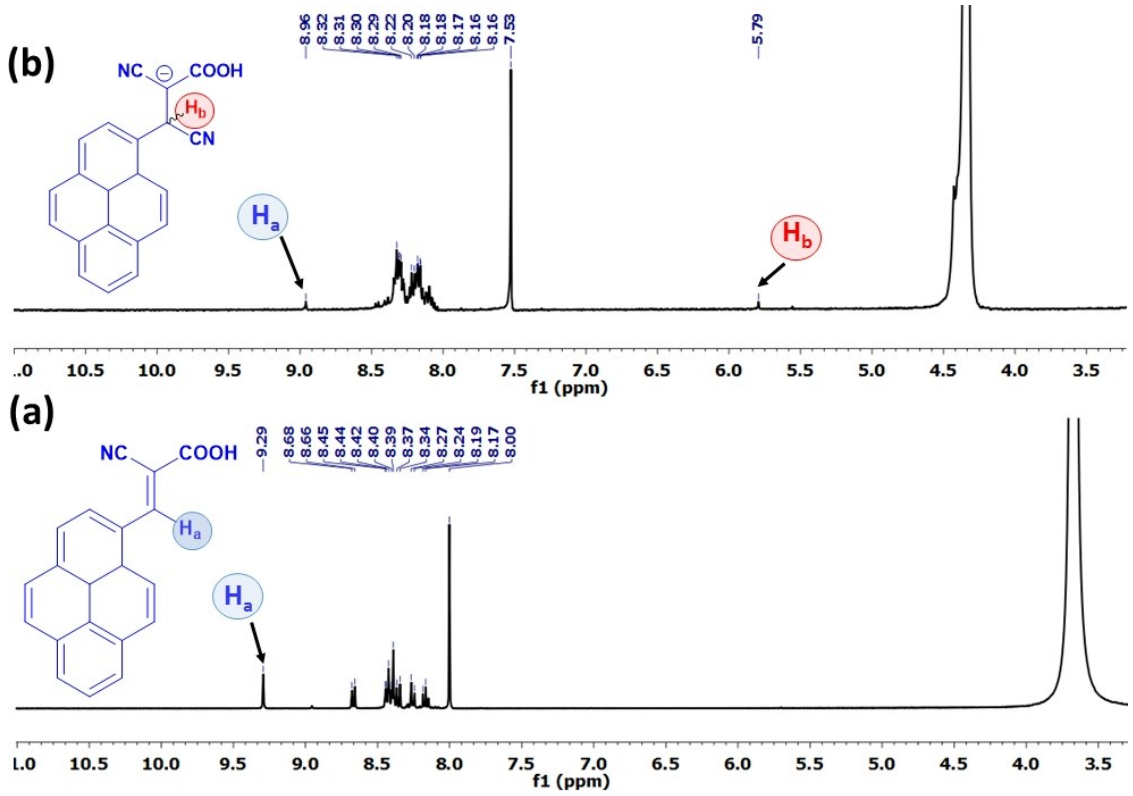

Figure S21. ^{1}H NMR spectrum of (a) **P-1'** and (b) cyanide treated **P-1'** digested in K_3PO_4/D_2O. The appearance of the new peak at 5.79 ppm in the ^{1}H NMR spectrum of cyanide treated **P-1'** supports the proposed nucleophilic addition of cyanide to the vinyl group of the pyrene moiety.

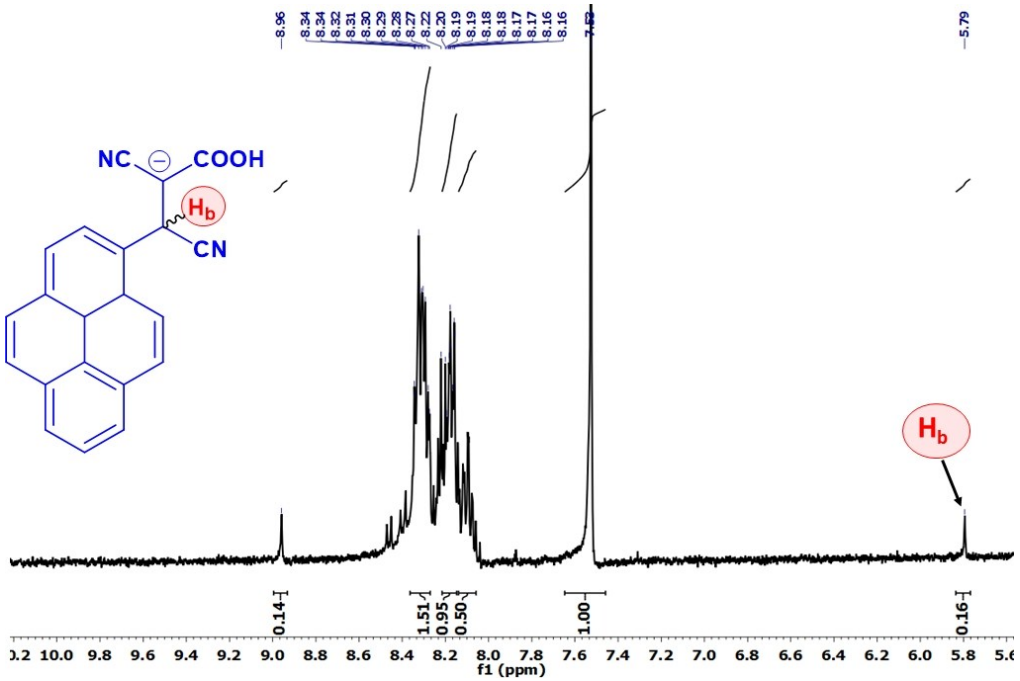

Figure S22. ^{1}H NMR spectrum of cyanide treated **P-1'** after digestion. The peaks corresponding to H_2TDC ligand were set to an integration of 1 and all new peaks were integrated accordingly. For cyanide treated **P-1'**, the new peak (H_b) at 5.79 ppm is approx. 0.16 with respect to protons of H_2TDC ligand. Due to nucleophilic attack of cyanide, the integration value of vinylic proton (H_a) decreases from ~ 0.30 to ~0.14. Hence, percentage conversion of incorporated CPAA ligand to its cyanide adduct is ~53% under sensing conditions.

References:

1. W.-W. He, G.-S. Yang, Y.-J. Tang, S.-L. Li, S.-R. Zhang, Z. M. Su and Y.-Q. Lan, *Chem. Eur. J.*, 2015, **21**, 9784-9789.
2. A. Kathiravan, M. Panneerselvam, K. Sundaravel, N. Pavithra, V. Srinivasan, S. Anandand and M. Jaccob, *Phys. Chem. Chem. Phys.*, 2016, **18**, 13332-13345
3. M. J. Frisch, G. W. Trucks, H. B. Schlegel, G. E. Scuseria, M. A. Robb, J. R. Cheeseman, G. Scalmani, V. Barone, B. Mennucci, G. A. Petersson, H. Nakatsuji, M. Caricato, X. Li, H. P. Hratchian, A. F. Izmaylov, J. Bloino, G. Zheng, J. L. Sonnenberg, M. Hada, M. Ehara, K. Toyota, R. Fukuda, J. Hasegawa, M. Ishida, T. Nakajima, Y. Honda, O. Kitao, H. Nakai, T. Vreven, J. J. A. Montgomery, J. E. Peralta, F. Ogliaro, M. Bearpark, J. J. Heyd, E. Brothers, K. N. Kudin, V. N. Staroverov, R. Kobayashi, J. Normand, K. Raghavachari, A. Rendell, J. C. Burant, S. S. Iyengar, J. Tomasi, M. Cossi, N. Rega, J. M. Millam, M. Klene, J. E. Knox, J. B. Cross, V. Bakken, C. Adamo, J. Jaramillo, R. Gomperts, R. E. Stratmann, O. Yazyev, A. J. Austin, R. Cammi, C. Pomelli, J. W. Ochterski, R. L. Martin, K. Morokuma, V. G. Zakrzewski, G. A. Voth, P. Salvador, J. J. Dannenberg, S. Dapprich, A. D. Daniels, O. Farkas, J. B. Foresman, J. V. Ortiz, J. Cioslowski and D. J. Fox, *Gaussian 09, Revision A.1.; Gaussian, Inc.: , Wallingford, CT*, 2009.
4. R. Dalapati, S. Nandi, H. Reinsch, B. K. Bhunia, B. B. Mandal, N. Stock and S. Biswas, *CrystEngComm*, 2018, **20**, 4194-4201.

5. A. Karmakar, N. Kumar, P. Samanta, A. V. Desai and S. K. Ghosh, *Chem. Eur.J.*, 2016, **22**, 864 -868.
6. A. Das and S. Biswas, *Sens. Actuators, B*, 2017, **250**, 121-131.
7. A. Karmakar, B. Joarder, A. Mallick, P. Samanta, A. V. Desai, S. Basu and S. K. Ghosh, *Chem. Commun.*, 2017, **53**, 1253-1256.
8. L. Wang, S. Wang and Y. Chen, *Microchim. Acta*, 2017, **184**, 4597-4602.
9. H. Fang, G. Cai, Y. Hu and J. Zhang, *Chem. Commun.*, 2018, **54**, 3045-3048.
10. S. Mondal, S. S. Ali, S. Manna, K. Maiti, M. R. Uddin, S. Mandal, D. Mandal and A. K. Mahapatra, *New J. Chem.*, 2017, **41**, 12581-12588.
11. K. H. Jung and K.-H. Lee, *Anal. Chem.*, 2015, **87**, 9308-9314.
12. A. Panja and K. Ghosh, *ChemistrySelect*, 2018, **3**, 1809-1814.
13. J. Li, J. Gao, W. W. Xiong, P. Z. Li, H. Zhang, Y. Zhao and Q. Zhang, *Chem. - Asian J.*, 2014, **9**, 121-125.
14. L. Lan, T. Li, T. Wei, H. Pang, T. Sun, E. Wang, H. Liu and Q. Niu, *Spectrochim. Acta, Part A*, 2018, **193**, 289-296.
15. L. Tian, Y. Li, T. Ren, Y. Tong, B. Yang and Y. Li, *Talanta*, 2017, **170**, 530-539.
16. C.-F. Chow, M. H. Lam and W.-Y. Wong, *Inorg. Chem.*, 2004, **43**, 8387-8393.
17. K. Keshav, P. Torawane, M. K. Kumawat, K. Tayade, S. K. Sahoo, R. Srivastava and A. Kuwar, *Biosens. Bioelectron.*, 2017, **92**, 95-100.
18. Q. Lin, K.-P. Zhong, J.-H. Zhu, L. Ding, J.-X. Su, H. Yao, T.-B. Wei and Y.-M. Zhang, *Macromolecules*, 2017, **50**, 7863-7871.